Published in final edited form as:
Neuroscience. 2010 June 16; 168(1): 31–47. doi:10.1016/j.neuroscience.2010.03.036.

Intrinsic Membrane Properties of Pre-oromotor Neurons in the Intermediate Zone of the Medullary Reticular Formation

Sharmila Venugopal[1], **Jack A. Boulant**[2], **Zhixiong Chen**[3], and **Joseph B. Travers**[3]

[1] Center for Adaptive Neural Systems, Arizona State University

[2] Dept. of Physiology and Cell Biology, Ohio State University

[3] Division of Oral Biology, Ohio State University

Abstract

Neurons in the lower brainstem that control consummatory behavior are widely distributed in the reticular formation (RF) of the pons and medulla. The intrinsic membrane properties of neurons within this distributed system shape complex excitatory and inhibitory inputs from both orosensory and central structures implicated in homeostatic control to produce coordinated oromotor patterns. The current study explored the intrinsic membrane properties of neurons in the intermediate subdivision of the medullary reticular formation (IRt). Neurons in the IRt receive input from the overlying (gustatory) nucleus of the solitary tract and project to the oromotor nuclei. Recent behavioral pharmacology studies as well as computational modeling suggest that inhibition in the IRt plays an important role in the transition from a taste-initiated oromotor pattern of ingestion to one of rejection. The present study explored the impact of hyperpolarization on membrane properties. In response to depolarization, neurons responded with either a tonic discharge, an irregular/burst pattern or were spike-adaptive. A hyperpolarizing pre-pulse modulated the excitability of most (82%) IRt neurons to subsequent depolarization. Instances of both increased (30%) and decreased (52%) excitability were observed. Currents induced by the hyperpolarization included an outward 4-AP sensitive K^+ current that suppressed excitability and an inward cation current that increased excitability. These currents are also present in other subpopulations of RF neurons that influence the oromotor nuclei and we discuss how these currents could alter ring characteristics to impact pattern generation.

Keywords

ingestion; oromotor; taste; pattern generation

Introduction

Neurons directly controlling oromotor behavior are widely distributed in the lower brainstem. This substrate is considered sufficient for the generation of consummatory oral rhythmic function because midbrain decerebrate preparations can chew, lick and swallow (Miller and Sherrington, 1916, Grill and Norgren, 1978). Moreover, these behaviors are conceptualized as originating from central pattern generators (CPG) because each can be elicited following

Corresponding author: Joseph Travers, 305 W 12th Ave, Columbus, OH 43210, (614) 292 6365, travers.1@osu.edu.

central stimulation in the absence of peripheral feedback (Sumi, 1970, Dellow and Lund, 1971). Although the CPG for swallowing has been localized to the caudal medulla, reviewed in (Jean, 2001), the substrate for licking and mastication has been somewhat more elusive. Various regions of the reticular formation (RF) and orosensory nuclei have been proposed as part of this circuitry including the mesencephalic trigeminal nucleus (Del Negro and Chandler, 1997, Wu et al., 2001, Tanaka et al., 2003), principal trigeminal nucleus (Tsuboi et al., 2003, Brocard et al., 2006), supratrigeminal nucleus (Hsiao et al., 2007) and parvocellular RF just caudal to the motor trigeminal nucleus (Min et al., 2003). It is likely, however, that this circuitry also extends caudal to the pons. Other studies have provided strong evidence for a role of the medullary RF in consummatory oromotor behavior including nucleus gigantocellularis and laterally-adjacent neurons in the intermediate reticular zone (IRt) (Nozaki et al., 1986, Chen et al., 2001, Nakamura et al., 2004).

The IRt may be particularly important in adjusting oromotor behavior in response to the chemical constituents of foods and liquids (Travers et al., 1997). Pharmacological inactivation of the IRt with $GABA_A$ agonists or glutamate antagonists not only suppresses licking (ingestion) in response to preferred stimuli like sucrose, but also gaping (rejection) in response to aversive compounds such as quinine (Chen et al., 2001, Chen and Travers, 2003). Furthermore, the IRt contains a large number of neurons with direct projections to the oromotor nuclei (Holstege et al., 1977, Travers and Norgren, 1983) and receives local gustatory and oral somatosensory input from brainstem structures (Herbert et al., 1990, Halsell et al., 1996, Dauvergne et al., 2001, Zerari-Mailly et al., 2001), as well as forebrain projections from areas involved in the homeostatic control of ingestive behavior (Valverde, 1962, Shammah-Lagnado et al., 1992, Travers et al., 1997). Some excitatory and inhibitory inputs to the IRt have been identified. Excitatory inputs to IRt pre-oromotor neurons include a glutamatergic projection from the overlying rostral (gustatory) nucleus of the solitary tract gustatory (rNST) to pre-hypoglossal neurons (Nasse et al., 2008). Similarly, there is evidence for a glutamatergic hypothalamic projection to identified pre-motor trigeminal neurons (Notsu et al., 2008). Inhibitory inputs include indirect (polysynaptic) GABAergic inputs to IRt pre-hypoglossal neurons from the rNST (Nasse et al., 2008) and forebrain GABAergic inputs from the amygdala (Jongen-Relo and Amaral, 1998, Cassell et al., 2003).

Membrane properties are crucial in transforming excitatory and inhibitory synaptic inputs to produce patterned output in CPG's. However, in contrast to neurons in the pons, virtually nothing is known of the intrinsic membrane properties of IRt neurons. Pontine RF neurons involved with oromotor function comprise a heterogeneous population consisting of cells that respond with tonic, phasic, bursting, or spike-adaptive firing patterns in response to membrane depolarization (Min et al., 2003, Hsiao et al., 2007). Hyperpolarization-induced currents include both an inward cation current (I_h), or pacemaker current (Pape, 1996, Robinson and Siegelbaum, 2003, Wahl-Schott and Biel, 2009), and a transient outward potassium current (Min et al., 2003, Birnbaum et al., 2004, Hsiao et al., 2007). Both currents are implicated in pattern generation but have opposite effects on membrane excitability, conferring the ability to affect complex transformations in neural output (Funahashi et al., 2002a, Harris-Warrick, 2002, Burdakov, 2005, MacLean et al., 2005). Hyperpolarization-induced currents are of particular interest in the IRt, since inhibition in this substrate has been hypothesized to be part of the mechanism that underlies the dramatic change in oral motor responses to preferred versus avoided tastes (Chen et al., 2001, Chen and Travers, 2003, Venugopal et al., 2007, Nasse et al., 2008).

In the present study, we used whole cell patch clamp recordings to identify different neuron types in the IRt. In response to depolarization, most neurons displayed a pattern of tonic discharge. However, some neurons displayed irregular spike trains or bursts of spikes and others were spike-adaptive. Many neurons also exhibited modulation of excitability in response

to a hyperpolarizing pre-pulse. Under voltage-clamp, we show the presence of a hyperpolarization-activated inward cation current (I_h) and outward transient current (TOC) and discuss how these currents could influence the ring characteristics of a neuron involved in oromotor pattern generation.

Experimental Procedures

Whole cell recording was performed from brainstem slices of 45 neonatal Sprague-Dawley rats (P8-P12). In a subset of preparations (n = 33), neurons were identified as pre-hypoglossal by first injecting a retrograde tracer into the hypoglossal nucleus (mXII). To make the injections, rat pups were injected with glycopyrrolate (sc: 0.02 mg/kg) to prevent excess pulmonary mucus secretion and then deeply anesthetized with a combination of Ketamine and Xylazine (ip: 90/30 mg/kg). The pups were gently placed in a stereotaxic frame and held in place with mouse ear-bars. A midline incision was made through the skin and the foramen magnum opened to expose the caudal medulla at the level of the area postrema. Injections into the hypoglossal nucleus were made 0.2 mm rostral to obex and 0.2 mm lateral to the midline. The depth was determined by observing microstimulation-induced lingual movements elicited with a micropipette (tip diameter 20–40 μm) filled with 0.9% saline (Nasse et al., 2008). The saline pipette was removed and replaced with a micropipette filled with Rhodamine-labeled fluorescent microspheres, (0.04 μm diameter: Invitrogen, Carlsbad, CA). Fifty to 150nl of fluorescent microspheres were injected, the pipette was left in place for 10–20 minutes and removed. The incision was closed with 4.0 braided sutures and a drop of cyanoacrylate glue was placed on the exposed end of the sutures to prevent the Dam from removing them. Rat pups were returned to their home cage where they survived 12–72 hrs to allow retrograde transport of the fluorescent tracer. All experimental protocols were approved by the Ohio State University Institutional Animal Care and Use Committee in accordance with guidelines from the National Institutes of Health.

Slice Preparation

One to three days post-injection, rat pups were decapitated under deep anesthesia (33% Urethane, 3 ml/kg). The skull was removed from a level extending from just rostral to lambda to the first cervical vertebrae and the brainstem extracted under continuous perfusion of a cooled (4°C), carboxygenated (95% O_2, 5% CO_2) modified Kreb's "cutting solution" containing (mM): 110 choline, 25 $NaHCO_3$, 3 KCl, 7 $MgSO_4$, 1.5 NaH_2PO_4, 10 d-Glucose, 0.5 $CaCl_2$. The brain was blocked ~1 mm caudal to obex and rostrally at the level of the incoming seventh nerve and glued to a ceramic block with cyanoacrylate for sectioning in the coronal plane (Vibratome model 1000, Vibratome, St. Louis, MO). Coronal sections (350 μm) cut with a sapphire knife were transferred to a warmed (32°C) incubation chamber and perfused with carboxygenated normal Kreb's solution (mM): 124 NaCl, 25 $NaHCO_3$, 3 KCl, 1 $MgSO_4$, 1.5 NaH_2PO_4, 10 d-glucose, 1.5 $CaCl_2$.

Whole Cell Recording

Following at least 1 hour incubation, a single slice was transferred to a custom recording chamber mounted on the stage (Syskiyou Instruments, Grants Pass, OR) of a microscope (Nikon E600FN). Brain slices were held in place by a custom-made gold harp fitted with nylon threads and continuously perfused with warmed (32°C) carboxygenated normal Kreb's solution (2 ml/min). Patch pipettes with a resistance of 4–6MΩ and tip diameter ≤1μm were formed from 1.5 mm thin wall borosilicate glass (A-M systems, Sequim, WA) pulled on a Narishige PP-83 vertical Pipette puller. The patch pipette solution consisted of (mM): 140 potassium gluconate, 10 EGTA, 10 Hepes, 1 $MgCl_2$, 1 $CaCl_2$, 2 ATP, and 5 NaCl. Lucifer yellow (0.1%) was added to the pipette solution to label recorded neurons for morphometric analysis and to determine location. Under IR-DIC and epifluorescent optics, patch pipettes

were guided to retrogradely labeled neurons within the RF (Fig. 1). Patch clamp recordings (Model 2400, AM Systems) were performed in whole cell configuration achieved by rupturing the neuronal membrane with intact gigaohm seal (resistance ≥1 GΩ).

Experimental protocols and measurements

A membrane resistance test was initially performed to determine neuron viability. Under current clamp, resistance was calculated as the slope of the line fitted to injected current (steps from −0.2 nA to 0 nA; step size = 0.05 nA) versus the corresponding membrane potential measured at the end of 250 ms. Membrane capacitance and time constant were obtained by a built-in voltage-clamp 2-pulse test (Axon Clampfit 9). The criteria for inclusion were a stable resting potential more negative than −40mV, an AP amplitude ≥40mV and membrane resistance ≥100M (Nasse et al., 2008). The action potential (AP) amplitude was measured as the difference in membrane potential from the threshold of the spike to the peak of the first AP to a 0.2 nA pulse. The resting membrane potential was monitored constantly to ensure stable membrane behavior and recordings that did not meet the above criteria were excluded from analysis.

Current Clamp Protocols

Following the membrane resistance test, current clamp protocols were used to classify neurons in response to depolarization and to determine whether a hyperpolarizing pre-pulse changed the cell's firing characteristics. Membrane sag and spike onset delay were also measured. Neurons were typically held at their resting membrane potential. For each neuron, the mean instantaneous frequency (MIF) was determined in response to (1) depolarization (1 s) at a current intensity of 1–3 times the threshold based on the membrane resistance test, and (2) depolarization preceded by a hyperpolarizing pre-pulse (−150 to −300pA; 500ms). The difference in the MIF with and without the hyperpolarizing pre-pulse and the difference in the number of action potentials during the 1 s depolarization were used as measures of hyperpolarization-induced changes in neuron excitability.

Membrane potential sag was measured as the difference in membrane voltage from the most negative value during the hyperpolarizing pulse to the value at the end of the pulse (Fig. 2A). A membrane sag of > 2 mV was used as the criterion to categorize cells with sag (Hsiao et al., 2007). The hyperpolarization-induced spike onset delay was calculated as the difference in latencies between the peaks of the first APs produced with and without a hyperpolarizing pre-pulse. In a subset of neurons, increasing steps of hyperpolarization (0 pA to −200 pA; step size = 50 pA) were used to determine the relationship between hyperpolarization and spike onset delay.

Voltage-clamp protocols and whole cell current measurements

A voltage-clamp protocol to test for the presence of a hyperpolarization-activated inward current (I_h) underlying membrane sag consisted of steps of hyperpolarizing test potentials (−40 mV to −100 mV; step size: 10 mV) for 1 s duration from a holding potential of −40 mV. The magnitude of inward current was measured as the area under the curve between the onset of the slow inward current and the end of the 1 s command voltage, with the current value at the end defined as baseline (Fig. 2B). In a subset of cells (n= 6), an organic blocker of non-specific cation channels ZD7288 was used to confirm the presence of the hyperpolarization-activated inward cation current I_h (BoSmith et al., 1993,Hogan and Poroli, 2008). In a subset of neurons (n = 12), the sensitivity of a transient K^+ current was tested with and without (0.1 – 1 mM) 4-aminopiridine (4-AP) in a bath solution containing 10 mM TEA (tetra ethyl ammonium) and 1 μM TTX (tetrodotoxin). Voltage dependency of activation was tested by holding the membrane potential at ~−90 mV and clamping to a series of test potentials from −90 to 0 mV. Peak outward current was plotted against the membrane potential and fit with a Boltzmann

equation (Clampfit 9). To determine if neurons received input from the rostral (gustatory) nucleus of the solitary tract (rNST), a stimulating electrode was placed in the rNST in a subset of preparations (n=20). Post-synaptic inward (excitatory), or outward (inhibitory) currents (Fig. 2C & D) evoked by 50 Hz trains were recorded under voltage-clamp mode with the membrane held near the resting potential (train duration 100 ms; 0.1 ms pulses; 100 pA – 150 pA).

Neuron reconstruction

Following recording, sections were stored in 10% Formalin for a minimum of 24 hrs. Slices were mounted on gelatin coated slides, dried, coated with Vecta Shield (Vector Laboratories, Burlingame, CA) and coverslipped. Lucifer Yellow filled cells were photographed through a Zeiss Axioscope-2 upright microscope under epifluorescence and Z-stacks constructed using Axioview software in 2.5 μm steps at 20X magnification and imported into Neurolucida (Microbrightfield, Williston, VT) for reconstruction. The locations of reconstructed neurons were plotted on standard sections and cell size (area), form factor, number of primary dendrites and total dendritic length calculated (NeuroExplorer: Microbrightfield, Williston, VT). In most cases, there was only one filled neuron on a given slice for reconstruction. In 3 instances, however, there were 2 labeled neurons which were then differentiated by matching the dendritic morphology from a photomicrograph made at the time of patching with the Z-stack photomicrographs.

Results

A total of 62 neurons met the criteria for inclusion. All were tested with the protocols used to establish changes in excitability due to a hyperpolarizing pre-pulse and were located in the medullary reticular formation subjacent to the rostral nucleus of the solitary tract (rNST) extending from the level where the NST is adjacent to the IVth ventricle to the rostral pole of the nucleus (Fig. 3). A large proportion projected to the hypoglossal nucleus (43/51 injected) and/or were activated by rNST stimulation (23/45 tested). Twelve of the neurons that did not respond to rNST stimulation were not assessed for their projection to mXII so their connectivity is uncertain, but they are included because they were in close proximity to the other RF neurons and shared similar membrane properties. Most responses to rNST stimulation were excitatory (58%), with fewer inhibitory (25%) or mixed (17%) (Fig 2C & D) responses. These proportions are similar to our previous report (Nasse et al., 2008).

Morphological Types

Neurons were classified morphologically, as has been done in similar studies of RF neurons (Min et al., 2003, Hsiao et al., 2007) as (1) fusiform, if they had an elongate appearance and primary dendrites emanating from both poles, (2) pyramidal, for cells with a triangular appearance and three primary dendrites, and (3) multipolar, if they had a more variable soma shape with four or more primary dendrites (Fig. 4). Table I summarizes these results and indicates that fusiform neurons differed significantly from multipolar neurons with more narrow profiles (form factor) and fewer primary dendrites. Although the area of the pyramidal neurons was nominally larger than either the fusiform or multipolar neurons (see Fig. 4), this difference did not achieve statistical significance. In 22 instances an axonal process could be identified. Axonal terminations could not be determined but in the majority of cases, the trajectory was in a medial direction (n=14). Some axons projected ventrally (n=4) or laterally (n=4) but none extended in a dorsal direction. Membrane properties of the 3 types of neurons did not differ (Table I).

Physiological Types

Neurons were classified into 3 types based on their response to a 1 s depolarization (Table 2: row 1). The most frequent response (39/62) was a tonic firing pattern with regular interspike

intervals (Fig 5B &C). Twelve neurons had irregular or burst patterns (Fig. 5D) and 11 showed a rapid spike adaptation with only 1 or 2 spikes (Fig. 5A). Except for neurons exhibiting spike adaptation, a hyperpolarizing pre-pulse altered the response to depolarization. These changes are summarized in Table 2 (row 2) which classifies neurons according to whether they showed an increase in excitability (E), a reduction in excitability (R) or no effect (NE). Excitability was defined as the difference in MIF elicited by the depolarizing pulse with and without the hyperpolarizing pre-pulse. R neurons were further subdivided into those that showed a delay in the onset of the first spike (R_D) following the hyperpolarizing pre-pulse (Fig. 5D) and those with no delay (R_{ND}) (Fig. 5C).

Hyperpolarization-induced changes in neuron excitability

Neurons with hyperpolarization-induced increased excitability (E neurons) were defined by their increase in MIF and corresponding spike count increase. The augmented excitability appeared uniform across the 1 s period of depolarization (Fig. 6). On average, spike count increased 74% following hyperpolarization (ANOVA, $p < .001$), but there was not a significant effect of time nor a time X treatment interaction. In a subset of E cells (n=14), we systematically tested a range of hyperpolarizing currents. Except in one case, the E cells tested showed monotonic increases in the MIF with hyperpolarization between 0 pA and −250 pA. For one cell however, there was a dramatic reversal at −150 pA such that the MIF was lower than without the hyperpolarizing pre-pulse.

The R neurons were divided into two subgroups based on the presence (R_D, n = 12) or absence (R_{ND}, n=20) of a hyperpolarization-induced delay in spike onset (Fig. 5C & D). These subgroups became even more differentiated with varying levels of hyperpolarization. There was a significant correlation between the degree of hyperpolarization and the magnitude of the delay in R_D neurons ($p=0.008$) whereas R_{ND} neurons never showed a delay regardless of the level of hyperpolarization (Fig. 7C). These two groups also differed in the magnitude of spike suppression (Fig. 6). R_{ND} neurons were more profoundly suppressed by pre-hyperpolarization (93.2% mean spike count reduction) compared to R_D cells which exhibited only a modest change in spike count (22% mean reduction). An ANOVA of R_{ND} neurons, revealed both treatment ($p < 0.001$) and time effects ($p < .037$) but the treatment X time interaction was not significant, consistent with a sustained depression of spikes with pre-hyperpolarization. An ANOVA of the R_D neurons revealed a significant treatment effect ($p=0.001$) and a treatment X time interaction ($p=0.009$). Post-hoc paired t-tests (non-adjusted) revealed a significant effect ($p=0.002$) only during the first interval. The reduction in mean spike count during the first interval is consistent with the delay in spike onset.

To determine if the reductions in excitability associated with a hyperpolarizing pre-pulse were a consistent cell characteristic, MIF was calculated for each step of hyperpolarizing current. Seven of 11 R_D neurons did show systematic decreases in the MIF with increasing degrees of hyperpolarization. In the remaining four cells, however, increases in hyperpolarization < −50pA produced more variable effects; notably, the MIF was sometimes greater than that produced by depolarization alone. These non-monotonic effects are indicative of interactions with other hyperpolarization-activated channels and are discussed below. Evaluating R_{ND} neurons at different levels of hyperpolarization was problematic due to the marked and long-lasting suppressions hyperpolarization produced in these cells. As evident from Table 2, the most common response of R_{ND} neurons to a hyperpolarizing pre-pulse was spike adaptation in which there was just 1 spike to depolarization (12/20). This profound suppression often outlasted the 1s test period and made it difficult for us to repeatedly test excitability changes. This sustained suppression was evident when a second depolarization was executed immediately following the protocol with the hyperpolarizing pre-pulse. In 6/7 cases, the second depolarization produced many fewer action potentials.

Overall, NE cells were less excitable compared to E and R neurons. Following a hyperpolarizing pre-pulse, 8/11 cells showed no change in spike count, with the remaining neurons responding with an increase (2/11 cells) or decrease (1/11 cells) by only 1 spike. The NE neurons remained invariant to depolarization with increasing steps of hyperpolarization. Several differences were noted in membrane properties among the three types of neurons classified according to changes in excitability (Table 3). Most of these differences were observed between E and NE neurons. Statistically significant differences were observed between these two classes of neurons in membrane resistance and time constant.

Hyperpolarization-induced sag and I_h

A prominent feature of many neurons was membrane voltage sag during the hyperpolarizing pre-pulse, e.g. figure 5B, C & D. Using a criterion of a 2 mV change in membrane voltage (Hsiao et al., 2007), sag was evident in 95% of E, 92% of R_D, 65% of R_{ND} and 46% of NE neurons. The average sag of NE neurons was lower than the other two groups ($p < .01$) (Table 3). Figure 8 shows an example of sag under both current (Fig. 8A) and voltage clamp (Fig. 8C), in a tonic neuron that showed a delay with a hyperpolarizing pre-pulse. Across a population of 12 neurons there was a high correlation ($r = 0.9$; $p < .001$) between the degree of sag (current clamp) and a slow inward current (voltage clamp) (Fig. 8E). Both membrane sag (Fig. 8B) and the inward current (Fig 8D) were blocked by ZD7288 (50 – 100 μM. On average, in 6 cells tested, ZD7288 blocked the slow inward current by 90%.

Hyperpolarization-induced transient outward current

The hyperpolarization-induced delay in spike onset is commonly attributed to a transient outward potassium current (I_A), e.g. (Dekin and Getting, 1987, Tell and Bradley, 1994). The same mechanism seems to account for the hyperpolarization-induced delay observed here. For example, figure 7A illustrates a delay neuron in which a series of hyperpolarizing current injections (0 to −200pA; step size=50pA) resulted in systematically increasing delay. Voltage-clamp recording in the same cell (Fig. 7B) shows a corresponding increase in the magnitude of the transient outward current with increasing hyperpolarization (−40 to −90 mV; step size=10 mV). Note that the length of the delay is proportional to the peak amplitude of the transient outward current. In 3 cells tested, the delay to a hyperpolarizing pre-pulse was reduced in the presence of 4-AP (Fig. 7D).

To characterize the transient outward current, a subset of neurons were tested under voltage-clamp in the presence of two widely used K^+ channel blockers: TEA and 4-AP (Del Negro and Chandler, 1997, Funahashi et al., 2002a, Jerng et al., 2004, Vydyanathan et al., 2005). Voltage-dependent outward currents were sensitive to both compounds. Subtracting the outward current remaining in the presence of 4-AP from the total outward current revealed a rapidly decaying transient outward current (Fig 9B). In 3 of the 6 neurons tested, the rate of decay of the 4-AP-sensitive outward current was fit with a single exponential (range: 50 – 278 ms). The time constant of the decay in the other 3 neurons was fit with a double exponential; the fast decay ranged from 4.8 – 55 ms, the slow decay from 71 – 454 ms (Fig. 9C). A TEA-sensitive current was also apparent which appeared as a voltage-dependent slow or non-inactivating outward current (Fig. 9B). Rapidly decaying transient outward currents sensitive to 4-AP were also evident when TEA was present in the bath. In these neurons (n=4), time constants were fit with single exponentials and ranged from 17.7 to 310 ms.

The voltage-dependent activation of I_A was examined with and without 4-AP and plotted as peak current (normalized) as a function of the membrane potential and the resulting curves fitted with the Boltzmann equation (Fig. 9D). In the presence of TTX and TEA, $V_{half\text{-}max}$ = −22 mV and Tau = 31.6 ms. When 4-AP was added, the corresponding values were −29mV and 92.8 ms. In the presence of TEA and 4-AP, the peak outward current evoked by a

hyperpolarizing pre-pulse followed by depolarization was reduced by 45.2 % compared to control values (paired t-test: $p < .05$). When TEA was not present in the bath, 4-AP was only slightly less effective with a mean reduction in the peak outward current by 43.5% (paired t-test, $p < .05$). Transient outward currents were found among all neuron types; of 20 neurons tested, there were 6 E, 6 R_D, 7 R_{ND} and 1 NE.

Interaction between hyperpolarization-induced membrane voltage sag and delay

All but one of the cells with hyperpolarization-induced delay also showed membrane sag, so it is not surprising, perhaps, that there was evidence for an interaction between I_h and I_A. Four neurons with both sag and delay showed evidence of such an interaction. Figure 10 illustrates a cell with both membrane sag and spike onset delay in response to a hyperpolarizing pre-pulse. Hyperpolarization induced with −300pA (Fig. 10B) produced greater sag and a shorter delay compared to a hyperpolarization induced with −200pA (Fig. 10A) which reduced sag concomitant with an increase in delay. Greater sag was also associated with an increase in the spike count during depolarization. This suggests an antagonistic interaction between the two ionic conductances. Similar observations were made in 3 other R_D cells where it was noted that hyperpolarization increased MIF over baseline level (0 pA) at certain levels of hyperpolarization rather than decreasing it.

Discussion

This study describes intrinsic membrane properties of neurons in the intermediate zone of the medullary reticular formation (IRt). The IRt has been implicated in oromotor behavior (Inoue et al., 1994, Travers et al., 1997), including taste-guided oromotor behavior (Chen et al., 2001, Chen and Travers, 2003) and we recorded from many neurons with direct projections to the hypoglossal nucleus as well as neurons receiving rostral (gustatory) NST input. Neurons in the IRt displayed heterogeneous intrinsic membrane properties that include a hyperpolarization-activated inward cation current (I_h), a current that often functions to increase neuronal excitability (Pape, 1996, Harris-Warrick, 2002), and a transient outward current (TOC) that reduces neuronal excitability (Birnbaum et al., 2004). Inhibition is thought to play an important role in the switch between ingestion and rejection (Chen and Travers, 2003, Venugopal et al., 2007, Nasse et al., 2008). Thus, by controlling neuron excitability, these hyperpolarization-induced currents can shape oromotor pattern formation. Neurons with similar membrane properties are also evident in other populations of RF neurons implicated in controlling oromotor behavior including the PCRt (Min et al., 2003) and supratrigeminal region (suV) (Hsiao et al., 2007). Together, with the medullary IRt, these neurons constitute a distributed RF substrate for the generation and coordination of oromotor function.

Neuronal types and ring properties

We recorded primarily from neurons dorsal in the IRt where pre-hypoglossal neurons are most numerous (Travers et al., 2005). These neurons are contiguous with, but caudal to those reported by Min et al. (Min et al., 2003) who recorded from pre-motor trigeminal neurons in the PCRt located between the exiting facial nerve and motor trigeminal nucleus. IRt neurons appeared somewhat larger (mean = (187 μM^3) compared to those in PCRt (mean = 167 μM^3) and could be further differentiated from their PCRt counterparts by their physiological properties. In particular, there were considerably fewer neurons with prominant bursting characteristics in the IRt (19%) compared to the PCRt (41%). Moreover, a qualitative inspection suggests that the degree of “burstiness” exhibited by PCRt cells is greater than that in IRt (compare Fig. 5D with Fig. 2 in (Min et al., 2003)). This conclusion is tentative since much longer depolarizations were used in PCRt. Indeed, in some instances, the first burst required 4s of depolarization although in other cases, bursts occurred within 1.5 s (Min et al., 2003). Because our depolarization protocol did not extend beyond 1 s, we may have missed

some bursting activity. Bursting in PCRt neurons was attributed to a low threshold, voltage-dependent Ca^{2+} channel that may also interact with I_h (Min et al., 2003). In contrast, neurons with bursting characteristics reported in suV (10%) were dependent on a riluzole-blockable persistent sodium channel (Hsiao et al., 2007). The present study did not explore the underlying mechanism for bursting, but we did note the absence of plateau potentials as reported in suV neurons.

Spike-adapting neurons in which depolarization elicited only one or two spikes were also observed in IRt (19%), PCRt (10%) (Min et al., 2003) and suV (8%) (Hsiao et al., 2007). These rapidly adapting responses were attibuted to a low-threshold, 4-AP sensitive K^+ current in mesencephalic neurons (Del Negro and Chandler, 1997) and a calcium activated K^+ current in PCRt neurons (Min et al., 2003). Spike-adapting neurons may also indicate an immature neuron; for example, many fewer spike-adaptive neurons were observed in the principal sensory trigeminal nucleus after P13 compared to younger pups (Brocard et al., 2006). Neurons with depolarization-induced tonic discharge were the most common type in all three RF regions: 63% IRt, 49% PCRt, 40% suV. Tonic neurons in IRt appeared similar to tonic suV neurons in that there was significantly more sag compared to spike adaptive neurons.

Hyperpolarization-induced cationic currents

In response to a hyperpolarizing pre-pulse, the firing patterns of most IRt neurons were altered. These changes can be partially explained by the presence of two hyperpolarizing-induced cationic currents. A sag potential elicited by the hyperpolarizing pre-pulse was evident in the majority of IRt neurons. A hyperpolarization-induced inward cation current (I_h) underlies sag potential (Pape, 1996), and we used a well known organic blocker, ZD7288 to successfully block the sag potential and I_h (Bennett et al., 2000, Ghamari-Langroudi and Bourque, 2000, Wilson, 2005). As with other reports, it was difficult to reverse the drug effects, even with a sustained washout (Mironov et al., 2000, Thoby-Brisson et al., 2000).

A voltage-dependent transient outward current (TOC) was also noted in many cells and was present in all neuron types encountered. The rapid decay and sensitivity to 4-AP suggests an A-type potassium current (Connor and Stevens, 1971b, Connor and Stevens, 1971a, Ammar et al., 2000, Jerng et al., 2004). The decay rate of the 4-AP sensitive outward current ranged from 18 ms to 310 ms, although in several instances, decay rates were better fit with two exponentials that included a fast and slow component. Other studies have reported similar results. In the area postrema, for example, neurons appeared to express either a fast or a slow outward current (Funahashi et al., 2002b). However, in the mesencephalic trigeminal nucleus (Negro and Chandler, 1997), nodose (McFarlane and Cooper, 1991) and dorsal root ganglion (Vydyanathan et al., 2005), neurons expressed both a fast and a slow TOC. The wide range of decay kinetics of K^+ mediated outward currents reported can be attributed to the differential expression of Kv subunits (Jerng et al., 2004, Vacher et al., 2008).

We relied primarily on pharmacologic tests to identify TOCs. Although both TEA and 4-AP are used widely to dissociate K^+ currents (Jerng et al., 2004, Vydyanathan et al., 2005), they are not entirely specific. Several studies, for example have reported the attenuation of TOC with TEA at 10 mM or higher (McFarlane and Cooper, 1991, Denton and Leiter, 2002), and 4-AP did not reduce a fast TOC induced in mesencephalic trigeminal neurons (Del Negro and Chandler, 1997). In IRt neurons, however, 4-AP reduced the peak TOC, regardless of whether 10 mM TEA was in the bath or not, consistent with other studies showing no effect of TEA on TOCs at 20 mM (Funahashi et al., 2002b, Vydyanathan et al., 2005).

In addition to its effect on transient K^+ channels, 4-AP also affects other types of ion currents including a sustained outward K+ current (Del Negro and Chandler, 1997) and calcium activated K^+ channels as indicated by 4-AP suppression of the after hyperpolarization potential

(AHP) (Nedergaard, 1999, Wilson et al., 2002, Cavelier et al., 2003). In fact, similar effects on AHP were observed in the present study (Fig 7D & E).

Despite the limitations imposed by pharmacological dissection, the $V_{half\text{-}max}$ for the TOC (−22 mV) was similar to that reported for other brainstem neurons, e.g. area postrema and trigeminal motor neurons (Hsiao and Chandler, 1995, Funahashi et al., 2002a). This TOC contributes to the delay in the first spike in a subset of neurons and both the TOC and the delay were suppressed by 4-AP, consistent with other reports (Tell and Bradley, 1994, Hsiao et al., 2007). A more complete characterization of TOCs in IRt neurons awaits experimental approaches less reliant on pharmacological dissection..

Changes in excitability

In response to a hyperpolarizing pre-pulse, the firing patterns of IRt neurons were recategorized into three groups: (1) increased excitability (E), (2) reduced excitability (R) with delay and no-delay, and (3) no effect (NE). For most neurons, classification remained invariant across multiple levels of hyperpolarization.

Although neurons could conveniently be classified into types based on changes in excitability, Figure 11, which ranks cells by the magnitudes of hyperpolarization-induced changes in excitability, suggests that they form a continuum. Sag was distributed across the population; however neurons with increased excitability showed significantly more sag compared to NE neurons, and tended toward more sag (27%) compared to R neurons. This is similar to suV where it was noted that spike adaptive neurons had less sag (Hsiao et al., 2007). All 11 of our NE neurons were spike-adaptive. As a population, suV neurons with sag exhibited only a marginal increase in postinhibitory rebound, i.e. increased excitability, compared to cells without sag. Similarly, we did not find a significant correlation between the degree of sag and changes in mean instantaneous frequency (excitability) in IRt. Thus, although I_h appears to contribute to an increase in excitability following hyperpolarization, other currents must be involved. For example, I_h may interact with the other sub-threshold mechanisms such as the persistent sodium current as seen in the trigeminal Mes V neurons (Wu et al., 2001) or T-type calcium currents (Bradley and Sweazey, 1992).

Interactions between I_h and I_A may also partially explain excitability differences among IRt neurons. On average, in neurons showing delay, increases in hyperpolarization resulted in increased delay (Fig. 7). However, figure 10 shows an instance where increased hyperpolarization resulted in a decreased delay and this shorter delay was accompanied by increased sag. Presumably, the increased inward current through HCN counteracted the transient outward potassium current in this neuron. We noted several other instances among delay neurons where the mean instantaneous frequency increased at higher levels of hyperpolarization, suggesting the superseding influence of I_h. Other studies have reported coincidence and interactions between I_h and I_A, (Funahashi et al., 2002a,Burdakov, 2005,MacLean et al., 2005). Although we observed the presence of a transient outward current, likely I_A, in six E cells, none exhibited delay. Thus, I_h alone or in conjunction with other inward currents, seems to overcome the reduction in excitability that might be expected with I_A.

Functional Significance

Based on pharmacological inactivation in adult rats, the IRt plays an important role in ororhythmic consummatory behavior (Chen et al., 2001, Chen and Travers, 2003). Although the present experiments were performed in animals P7 - P12, these animals are competent to perform gustatory discriminations and make oromotor responses of ingestion and rejection similar to adult animals, i.e. when a sweet gustatory stimulus is place in the mouth, they make small licking ingestive movements in contrast to the oral (gape) rejection response elicited by

a bitter stimulus such as quinine (Ganchrow et al., 1986, Nasse et al., 2008). Other studies suggest that the complete masticatory pattern does not emerge until around P12 (Westneat and Hall, 1992); however, simple rhythmic jaw movements can be observed even in embryonic rats (Narayanan et al., 1971).

Despite the sensori-motor competence of P7-P12 rats, neurons in the IRt are still likely immature. In fact, rats were selected at this age because the low level of myelination allowed neuron identification under differential interference contrast optics. This period, however is a time of rapid development and neither I_A nor I_h are necessarily mature. Although numerous studies report I_A in neonatal rats, an adult expression may not be present (Costa et al., 1994, Hattori et al., 2003, Deng et al., 2004, Walsh et al., 2009). Likewise, I_h can appear adult-like in some juvenile rat neurons (Richter et al., 1997) but not others (Tanaka et al., 2003, Rocha et al., 2006).

The present evidence suggests that the IRt is less likely to constitute a “rhythm” generating substrate than the pons. Neurons with more prominent intrinsic bursting characteristics occur in PCRt pars alpha just caudal to mV (Min et al., 2003), the supratrigeminal nucleus (Hsiao et al., 2007), the principal sensory trigeminal nucleus (Tsuboi et al., 2003, Brocard et al., 2006) and the mesencephalic trigeminal nucleus (Del Negro and Chandler, 1997, Wu et al., 2001, Tanaka et al., 2003). Indeed, even the motor trigeminal nucleus produces bursting activity in the presence of 5-HT (Hsiao et al., 1998). In contrast, although some IRt neurons were “irregular/bursting”, the incidence and degree of bursts of spikes appeared less than that associated with pontine cells, although a firm conclusion requires further investigation. Likewise, the currents identified in IRt, I_h and I_A, though implicated in rhythm generating circuits in other systems (Harris-Warrick, 2002), are not directly implicated in the burst generation in IRt. As evident from figure 5 a bursting neuron became more irregular with a hyperpolarizing pre-pulse. Admittedly, we also observed the opposite in at least one instance, i.e. a neuron with irregular activity became more rhythmic with the pre-pulse. Nevertheless, in IRt, I_A and I_h may play other important roles in motor pattern formation.

Behavioral pharmacological experiments demonstrate that infusions of a $GABA_A$ antagonist into the IRt changes sucrose-elicited small amplitude EMG licking responses into large amplitude EMG responses resembling quinine-evoked gapes (Chen and Travers, 2003). This effect suggests that disinhibition could be part of a switching mechanism between ingestion and rejection. Thus, one possible role of I_h in IRt might be to enhance excitability in a subpopulation of neurons upon the removal of inhibition (Nasse et al., 2008). I_h influences motor patterns in a number of systems including a feeding pattern generator in the crustacean stomatogastric ganglion (Harris-Warrick et al., 1995) and rhythmic activity in lumbar motoneurons of mice (Bertrand and Cazalets, 1998).

I_A also plays a role in motor pattern formation. In the caudal NST, for example, I_A has been proposed to mediate the phase delay controlling the peristaltic action of a pattern generator for swallowing (Jean, 2001). We can only speculate that the role of delay in the IRt may be to control the orderly recruitment of motoneurons to ensure a smooth, continuous movement. Single unit recording in the hypoglossal nucleus, for example, shows a continuous recruitment of motoneurons at different phases of the lick cycle (Travers and Jackson, 1992). Thus, variable degrees of I_A expression in a network of lingual protrudor and lingual retractor pre-motor neurons might ensure an orderly sequential firing of motor units. Indeed, one might expand this argument to the whole population of IRt neurons and suggest that the continuum of excitability evident in figure 11 reflects the role of hyperpolarization (inhibition) in ensuring an orderly, progressive firing of pre-motor neurons. Such a continuum may derive from IRt neurons with varying degrees of HCN and other hyperpolarizing-activated channels supporting competing inward and outward currents.

Acknowledgments

This work was supported by NIH DIC-00417. The authors thank Ken Herman, Saneeka Patel, Xiaodan Lin and Alex Dahm for technical assistance and Susan Travers for editing. This work was submitted in partial fulfillment of the requirements for a Ph.D. in Neuroscience at The Ohio State University (SV).

Abbreviations

4-AP	4-aminopyridine
AP	action potential
CPG	central pattern generator
E	cells with enhanced excitability due to pre-hyperpolarization
HCN	hyperpolarization-activated cation channel
I_A	transient outward potassium current
I_h	hyperpolarization-activated inward cation current
IRt	intermediate zone of the reticular formation
IV	fourth ventricle
mXII	hypoglossal nucleus
MIF	mean instantaneous frequency
NE	cells with no change in excitability
PCRt	parvocellular reticular formation
rNST	rostral nucleus of the solitary tract
R	cells with reduced excitability
R_D	subset of R cells with delay in spike onset
R_{ND}	subset of R cells with no delay in spike onset
RMP	resting membrane potential
RF	reticular formation
SuV	supratrigeminal nucleus
t	solitary tract
TEA	tetra ethyl ammonium
TTX	tetrodotoxin
TOC	transient outward current
ZD7288	4-ethylphenylamino-1,2- dimethyl-6-methylaminopyrimidinium chloride

References

Ammar AA, Sederholm F, Saito TR, Scheurink AJ, Johnson AE, Sodersten P. NPY-leptin: opposing effects on appetitive and consummatory ingestive behavior and sexual behavior. Am J Physiol Regul Integr Comp Physiol 2000;278:R1627–1633. [PubMed: 10848532]

Bennett BD, Callaway JC, Wilson CJ. Intrinsic membrane properties underlying spontaneous tonic firing in neostriatal cholinergic interneurons. J Neurosci 2000;20:8493–8503. [PubMed: 11069957]

Bertrand S, Cazalets JR. Postinhibitory rebound during locomotor-like activity in neonatal rat motoneurons in vitro. J Neurophysiol 1998;79:342–351. [PubMed: 9425203]

Birnbaum SG, Varga AW, Yuan LL, Anderson AE, Sweatt JD, Schrader LA. Structure and function of Kv4-family transient potassium channels. Physiol Rev 2004;84:803–833. [PubMed: 15269337]

BoSmith RE, Briggs I, Sturgess NC. Inhibitory actions of ZENECA ZD7288 on whole-cell hyperpolarization activated inward current (If) in guinea-pig dissociated sinoatrial node cells. Br J Pharmacol 1993;110:343–349. [PubMed: 7693281]

Bradley RM, Sweazey RD. Separation of neuron types in the gustatory zone of the nucleus tractus solitarii on the basis of intrinsic firing properties. J Neurophysiol 1992;67:1659–1668. [PubMed: 1629769]

Brocard F, Verdier D, Arsenault I, Lund JP, Kolta A. Emergence of intrinsic bursting in trigeminal sensory neurons parallels the acquisition of mastication in weanling rats. J Neurophysiol 2006;96:2410–2424. [PubMed: 16914618]

Burdakov D. Gain control by concerted changes in I(A) and I(H) conductances. Neural Comput 2005;17:991–995. [PubMed: 15881793]

Cassell MD, Gedney MT, Agassandian KA. Network architecture of central amygdala output shows strong connectional bias towards oro-lingual sensory and reflex circuits. Society for Neuroscience Abstracts 2003:594.10.

Cavelier P, Desplantez T, Beekenkamp H, Bossu JL. K+ channel activation and low-threshold Ca2+ spike of rat cerebellar Purkinje cells in vitro. Neuroreport 2003;14:167–171. [PubMed: 12598722]

Chen Z, Travers JB. Inactivation of amino acid receptors in medullary reticular formation modulates and suppresses ingestion and rejection responses in the awake rat. Am J Physiol Regul Integr Comp Physiol 2003;285:R68–83. [PubMed: 12663257]

Chen Z, Travers SP, Travers JB. Muscimol infusions in the brain stem reticular formation reversibly block ingestion in the awake rat. Am J Physiol Regul Integr Comp Physiol 2001;280:R1085–1094. [PubMed: 11247831]

Connor JA, Stevens CF. Prediction of repetitive firing behaviour from voltage clamp data on an isolated neurone soma. J Physiol 1971a;213:31–53. [PubMed: 5575343]

Connor JA, Stevens CF. Voltage clamp studies of a transient outward membrane current in gastropod neural somata. J Physiol 1971b;213:21–30. [PubMed: 5575340]

Costa PF, Santos AI, Ribeiro MA. Potassium currents in acutely isolated maturing rat hippocampal CA1 neurones. Brain Res Dev Brain Res 1994;83:216–223.

Dauvergne C, Pinganaud G, Buisseret P, Buisseret-Delmas C, Zerari-Mailly F. Reticular premotor neurons projecting to both facial and hypoglossal nuclei receive trigeminal afferents in rats. Neurosci Lett 2001;311:109–112. [PubMed: 11567790]

Dekin MS, Getting PA. In vitro characterization of neurons in the ventral part of the nucleus tractus solitarius. II. Ionic basis for repetitive firing patterns. J Neurophysiol 1987;58:215–229. [PubMed: 2441002]

Del Negro CA, Chandler SH. Physiological and theoretical analysis of K+ currents controlling discharge in neonatal rat mesencephalic trigeminal neurons. J Neurophysiol 1997;77:537–553. [PubMed: 9065827]

Dellow PG, Lund JP. Evidence for central timing of rhythmical mastication. J Physiol 1971;215:1–13. [PubMed: 5579653]

Deng P, Pang Z, Zhang Y, Xu ZC. Developmental changes of transient potassium currents in large aspiny neurons in the neostriatum. Brain Res Dev Brain Res 2004;153:97–107.

Denton JS, Leiter JC. Anomalous effects of external TEA on permeation and gating of the A-type potassium current in H. aspersa neuronal somata. J Membr Biol 2002;190:17–28. [PubMed: 12422269]

Funahashi M, Mitoh Y, Matsuo R. Electrophysiological properties of the rat area postrema neurons displaying both the transient outward current and the hyperpolarization-activated inward current. Brain Res Bull 2002a;58:337–343. [PubMed: 12128161]

Funahashi M, Mitoh Y, Matsuo R. Two distinct types of transient outward currents in area postrema neurons in rat brain slices. Brain Res 2002b;942:31–45. [PubMed: 12031850]

Ganchrow JR, Steiner JE, Canetto S. Behavioral displays to gustatory stimuli in newborn rat pups. Dev Psychobiol 1986;19:163–174. [PubMed: 3709973]

Ghamari-Langroudi M, Bourque CW. Excitatory role of the hyperpolarization-activated inward current in phasic and tonic firing of rat supraoptic neurons. J Neurosci 2000;20:4855–4863. [PubMed: 10864942]

Grill HJ, Norgren R. The taste reactivity test. II. Mimetic responses to gustatory stimuli in chronic thalamic and chronic decerebrate rats. Brain Res 1978;143:281–297. [PubMed: 630410]

Halsell CB, Travers SP, Travers JB. Ascending and descending projections from the rostral nucleus of the solitary tract originate from separate neuronal populations. Neuroscience 1996;72:185–197. [PubMed: 8730716]

Harris-Warrick RM. Voltage-sensitive ion channels in rhythmic motor systems. Curr Opin Neurobiol 2002;12:646–651. [PubMed: 12490254]

Harris-Warrick RM, Coniglio LM, Levini RM, Gueron S, Guckenheimer J. Dopamine modulation of two subthreshold currents produces phase shifts in activity of an identified motoneuron. J Neurophysiol 1995;74:1404–1420. [PubMed: 8989381]

Hattori S, Murakami F, Song WJ. Quantitative relationship between Kv4.2 mRNA and A-type K+ current in rat striatal cholinergic interneurons during development. J Neurophysiol 2003;90:175–183. [PubMed: 12843309]

Herbert H, Moga MM, Saper CB. Connections of the parabrachial nucleus with the nucleus of the solitary tract and the medullary reticular formation in the rat. J Comp Neurol 1990;293:540–580. [PubMed: 1691748]

Hogan QH, Poroli M. Hyperpolarization-activated current (I(h)) contributes to excitability of primary sensory neurons in rats. Brain Res 2008;1207:102–110. [PubMed: 18377879]

Holstege G, Kuypers HG, Dekker JJ. The organization of the bulbar fibre connections to the trigeminal, facial and hypoglossal motor nuclei. II. An autoradiographic tracing study in cat. Brain 1977;100:264–286. [PubMed: 884485]

Hsiao CF, Chandler SH. Characteristics of a fast transient outward current in guinea pig trigeminal motoneurons. Brain Res 1995;695:217–226. [PubMed: 8556333]

Hsiao CF, Del Negro CA, Trueblood PR, Chandler SH. Ionic basis for serotonin-induced bistable membrane properties in guinea pig trigeminal motoneurons. J Neurophysiol 1998;79:2847–2856. [PubMed: 9636091]

Hsiao CF, Gougar K, Asai J, Chandler SH. Intrinsic membrane properties and morphological characteristics of interneurons in the rat supratrigeminal region. J Neurosci Res 2007;85:3673–3686. [PubMed: 17668857]

Inoue T, Chandler SH, Goldberg LJ. Neuropharmacological mechanisms underlying rhythmical discharge in trigeminal interneurons during fictive mastication. J Neurophysiol 1994;71:2061–2073. [PubMed: 7931502]

Jean A. Brain stem control of swallowing: neuronal network and cellular mechanisms. Physiol Rev 2001;81:929–969. [PubMed: 11274347]

Jerng HH, Pfaffinger PJ, Covarrubias M. Molecular physiology and modulation of somatodendritic A-type potassium channels. Mol Cell Neurosci 2004;27:343–369. [PubMed: 15555915]

Jongen-Relo AL, Amaral DG. Evidence for a GABAergic projection from the central nucleus of the amygdala to the brainstem of the macaque monkey: a combined retrograde tracing and in situ hybridization study. Eur J Neurosci 1998;10:2924–2933. [PubMed: 9758162]

MacLean JN, Zhang Y, Goeritz ML, Casey R, Oliva R, Guckenheimer J, Harris-Warrick RM. Activity-independent coregulation of IA and Ih in rhythmically active neurons. J Neurophysiol 2005;94:3601–3617. [PubMed: 16049145]

McFarlane S, Cooper E. Kinetics and voltage dependence of A-type currents on neonatal rat sensory neurons. J Neurophysiol 1991;66:1380–1391. [PubMed: 1761988]

Miller FR, Sherrington CS. Some observations on the buccopharyngeal stage of reflex deglutition in the cat. Q J Exp Physiol 1916;9:147–186.

Min MY, Hsu PC, Yang HW. The physiological and morphological characteristics of interneurons caudal to the trigeminal motor nucleus in rats. Eur J Neurosci 2003;18:2981–2998. [PubMed: 14656294]

Mironov SL, Langohr K, Richter DW. Hyperpolarization-activated current, Ih, in inspiratory brainstem neurons and its inhibition by hypoxia. Eur J Neurosci 2000;12:520–526. [PubMed: 10712631]

Nakamura Y, Katakura N, Nakajima M, Liu J. Rhythm generation for food-ingestive movements. Prog Brain Res 2004;143:97–103. [PubMed: 14653154]

Narayanan CH, Fox MW, Hamburger V. Prenatal development of spontaneous and evoked activity in the rat (Rattus norvegicus albinus). Behaviour 1971;40:100–134. [PubMed: 5157515]

Nasse J, Terman D, Venugopal S, Hermann G, Rogers R, Travers JB. Local circuit input to the medullary reticular formation from the rostral nucleus of the solitary tract. Am J Physiol Regul Integr Comp Physiol 2008;295:R1391–1408. [PubMed: 18716034]

Nedergaard S. Regulation of action potential size and excitability in substantia nigra compacta neurons: sensitivity to 4-aminopyridine. J Neurophysiol 1999;82:2903–2913. [PubMed: 10601428]

Notsu K, Tsumori T, Yokota S, Sekine J, Yasui Y. Posterior lateral hypothalamic axon terminals are in contact with trigeminal premotor neurons in the parvicellular reticular formation of the rat medulla oblongata. Brain Res 2008;1244:71–81. [PubMed: 18948090]

Nozaki S, Iriki A, Nakamura Y. Localization of central rhythm generator involved in cortically induced rhythmical masticatory jaw-opening movement in the guinea pig. J Neurophysiol 1986;55:806–825. [PubMed: 3517246]

Pape HC. Queer current and pacemaker: the hyperpolarization-activated cation current in neurons. Annu Rev Physiol 1996;58:299–327. [PubMed: 8815797]

Richter H, Klee R, Heinemann U, Eder C. Developmental changes of inward rectifier currents in neurons of the rat entorhinal cortex. Neurosci Lett 1997;228:139–141. [PubMed: 9209118]

Robinson RB, Siegelbaum SA. Hyperpolarization-activated cation currents: from molecules to physiological function. Annu Rev Physiol 2003;65:453–480. [PubMed: 12471170]

Rocha N, Rolfs A, Strauss U. Ih is maturing: implications for neuronal development. Neurodegener Dis 2006;3:27–31. [PubMed: 16909033]

Shammah-Lagnado SJ, Costa MS, Ricardo JA. Afferent connections of the parvocellular reticular formation: a horseradish peroxidase study in the rat. Neuroscience 1992;50:403–425. [PubMed: 1279462]

Sumi T. Activity in single hypoglossal fibers during cortically induced swallowing and chewing in rabbits. Pflugers Arch 1970;314:329–346. [PubMed: 5461270]

Tanaka S, Wu N, Hsaio CF, Turman J Jr, Chandler SH. Development of inward rectification and control of membrane excitability in mesencephalic v neurons. J Neurophysiol 2003;89:1288–1298. [PubMed: 12612052]

Tell F, Bradley RM. Whole-cell analysis of ionic currents underlying the firing pattern of neurons in the gustatory zone of the nucleus tractus solitarii. J Neurophysiol 1994;71:479–492. [PubMed: 7513751]

Thoby-Brisson M, Telgkamp P, Ramirez JM. The role of the hyperpolarization-activated current in modulating rhythmic activity in the isolated respiratory network of mice. J Neurosci 2000;20:2994–3005. [PubMed: 10751452]

Travers JB, DiNardo LA, Karimnamazi H. Motor and premotor mechanisms of licking. Neurosci Biobehav Rev 1997;21:631–647. [PubMed: 9353796]

Travers JB, Jackson LM. Hypoglossal neural activity during licking and swallowing in the awake rat. J Neurophysiol 1992;67:1171–1184. [PubMed: 1597706]

Travers JB, Norgren R. Afferent projections to the oral motor nuclei in the rat. J Comp Neurol 1983;220:280–298. [PubMed: 6315785]

Travers JB, Yoo JE, Chandran R, Herman K, Travers SP. Neurotransmitter phenotypes of intermediate zone reticular formation projections to the motor trigeminal and hypoglossal nuclei in the rat. J Comp Neurol 2005;488:28–47. [PubMed: 15912497]

Tsuboi A, Kolta A, Chen CC, Lund JP. Neurons of the trigeminal main sensory nucleus participate in the generation of rhythmic motor patterns. Eur J Neurosci 2003;17:229–238. [PubMed: 12542659]

Vacher H, Mohapatra DP, Trimmer JS. Localization and targeting of voltage-dependent ion channels in mammalian central neurons. Physiol Rev 2008;88:1407–1447. [PubMed: 18923186]

Valverde F. Reticular formation of the albino rat's brain stem cytoarchitecture and corticofugal connections. J Comp Neurol 1962;119:25–53. [PubMed: 13924447]

Venugopal S, Travers JB, Terman DH. A computational model for motor pattern switching between taste-induced ingestion and rejection oromotor behaviors. J Comput Neurosci 2007;22:223–238. [PubMed: 17072755]

Vydyanathan A, Wu ZZ, Chen SR, Pan HL. A-type voltage-gated K+ currents influence firing properties of isolectin B4-positive but not isolectin B4-negative primary sensory neurons. J Neurophysiol 2005;93:3401–3409. [PubMed: 15647393]

Wahl-Schott C, Biel M. HCN channels: structure, cellular regulation and physiological function. Cell Mol Life Sci 2009;66:470–494. [PubMed: 18953682]

Walsh MA, Graham BA, Brichta AM, Callister RJ. Evidence for a critical period in the development of excitability and potassium currents in mouse lumbar superficial dorsal horn neurons. J Neurophysiol 2009;101:1800–1812. [PubMed: 19176612]

Westneat MW, Hall WG. Ontogeny of feeding motor patterns in infant rats: an electromyographic analysis of suckling and chewing. Behav Neurosci 1992;106:539–554. [PubMed: 1616619]

Wilson CJ. The mechanism of intrinsic amplification of hyperpolarizations and spontaneous bursting in striatal cholinergic interneurons. Neuron 2005;45:575–585. [PubMed: 15721243]

Wilson JM, Coderre E, Renaud LP, Spanswick D. Active and passive membrane properties of rat sympathetic preganglionic neurones innervating the adrenal medulla. J Physiol 2002;545:945–960. [PubMed: 12482898]

Wu N, Hsiao CF, Chandler SH. Membrane resonance and subthreshold membrane oscillations in mesencephalic V neurons: participants in burst generation. J Neurosci 2001;21:3729–3739. [PubMed: 11356860]

Zerari-Mailly F, Pinganaud G, Dauvergne C, Buisseret P, Buisseret-Delmas C. Trigemino-reticulo-facial and trigemino-reticulo-hypoglossal pathways in the rat. J Comp Neurol 2001;429:80–93. [PubMed: 11086291]

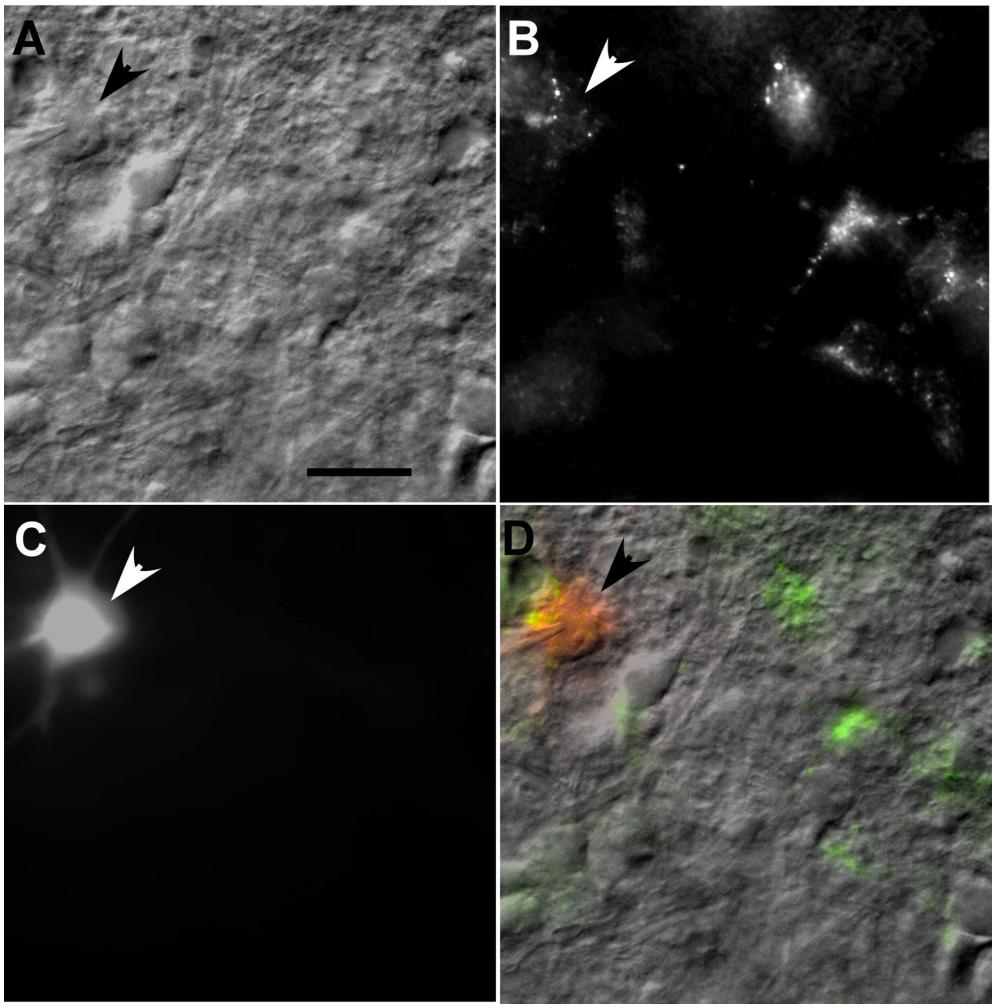

Figure 1.

A. Photomicrograph showing a patched RF neuron (arrow). The patch pipette tip is visible on the cell. B. The targeted neuron was retrogradely labeled and filled with Lucifer Yellow during recording (C). D. The overlay image of the patched neuron filled with the retrograde tracer and Lucifer Yellow. A stimulating electrode was place in the overlying rostral nucleus of the solitary tract (not shown). Scale bar 25 μm.

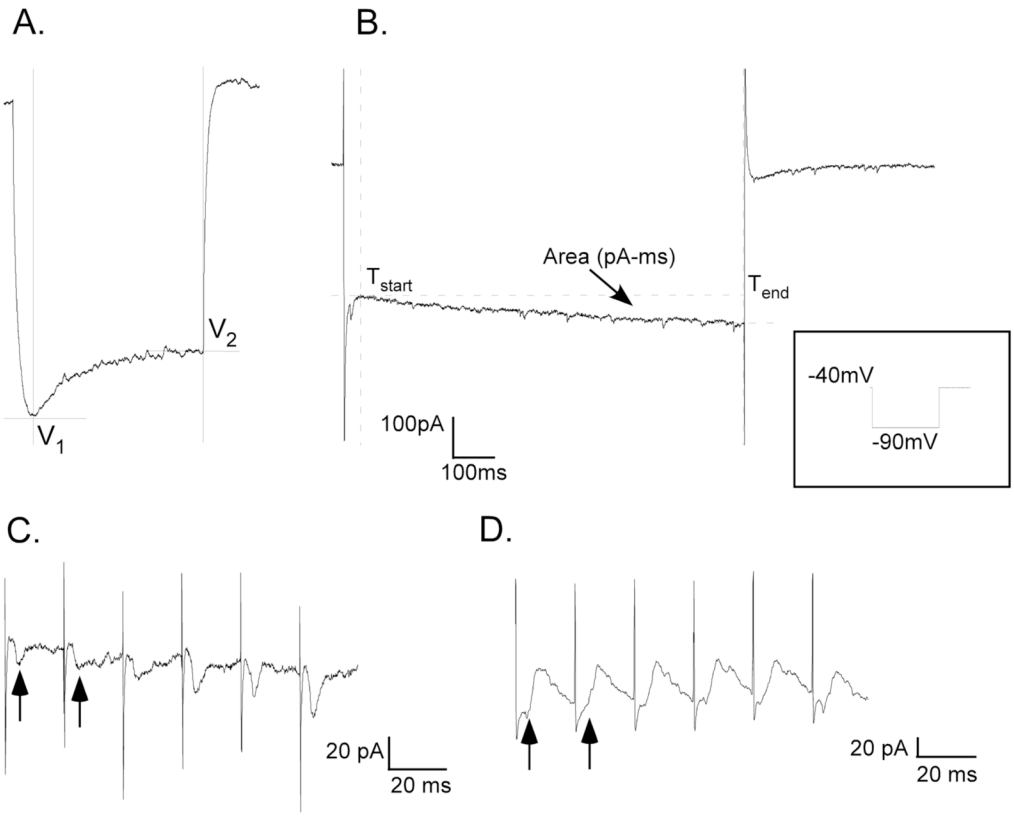

Figure 2.

A. Membrane voltage sag measurements: sag = $V_2 - V_1$, B. Voltage-clamp recording showing area measurement of slow inward current in response to protocol shown in inset. C. Stimulus-locked inward (excitatory) currents (arrows) evoked by train stimulation in a retrogradely labeled pre-motor IRt neuron. Average response to 10 replications of 50 Hz train, 0.1 ms pulse, 150 μA. D. Stimulus-locked outward (inhibitory) currents (arrows) in another retrogradely labeled IRt neuron. Average response to 10 replications of 50 Hz train, 0.1 ms pulse, 150 uA.

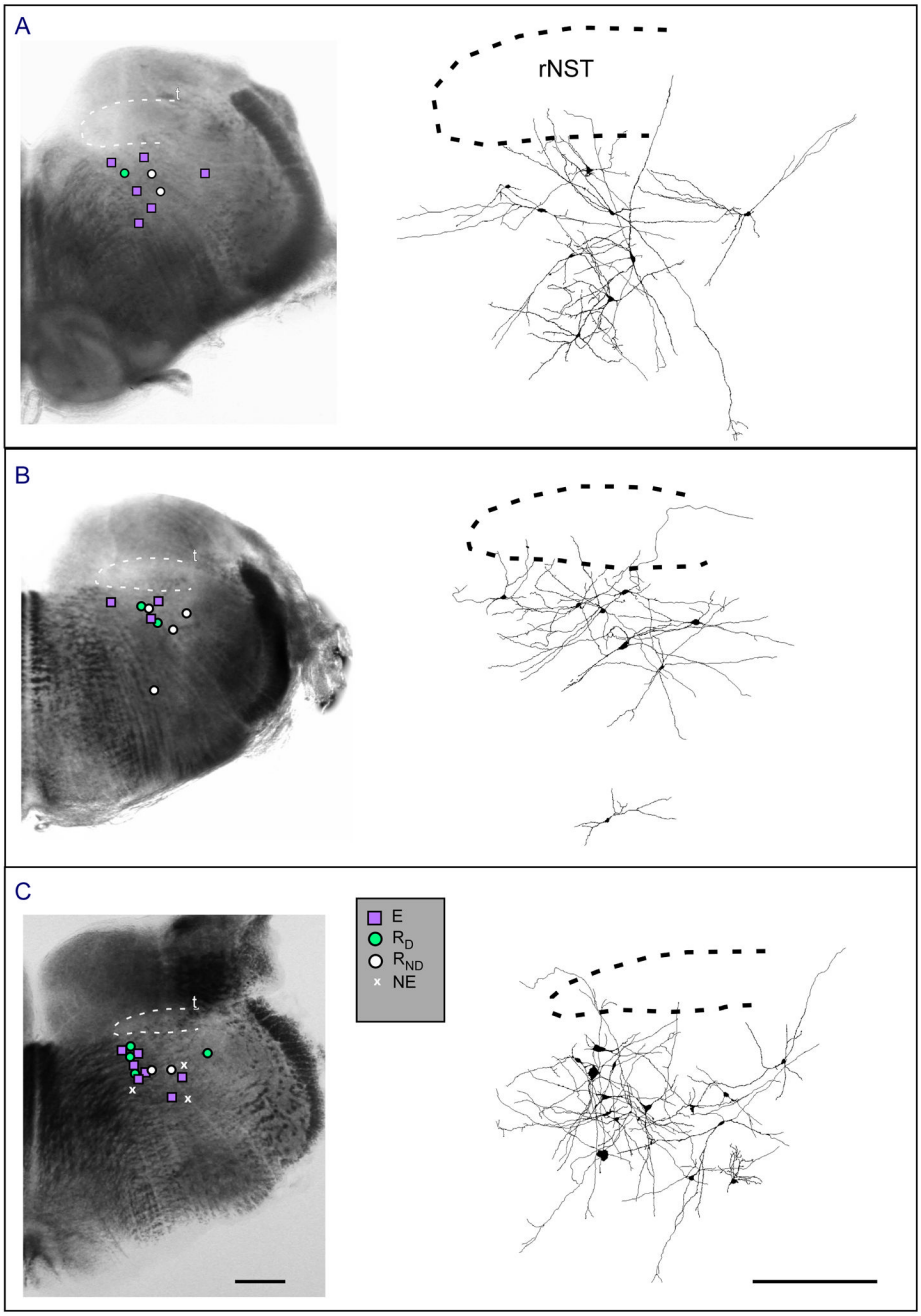

Figure 3.

Locations of patched neurons in the reticular formation subjacent to the rNST at three rostro-caudal levels. A is the most caudal, C is the most rostral. Photomicrographs on left with superimposed location of neurons categorized by excitability. Panels on right show reconstructed neurons with dendritic arborizations. Abbreviations: R_D, Reduced excitability with delay; E, increased excitability; R_{ND}, Reduced excitability with no delay; NE, no change in excitability; rNST, rostral nucleus of the solitary tract; T, solitary tract. Scale bar 0.5 mm.

Figure 4.
Morphological types of neurons in the intermediate zone of the reticular formation. From left to right: examples of fusiform, pyramidal, and multipolar neurons. Scale bar=20 μm.

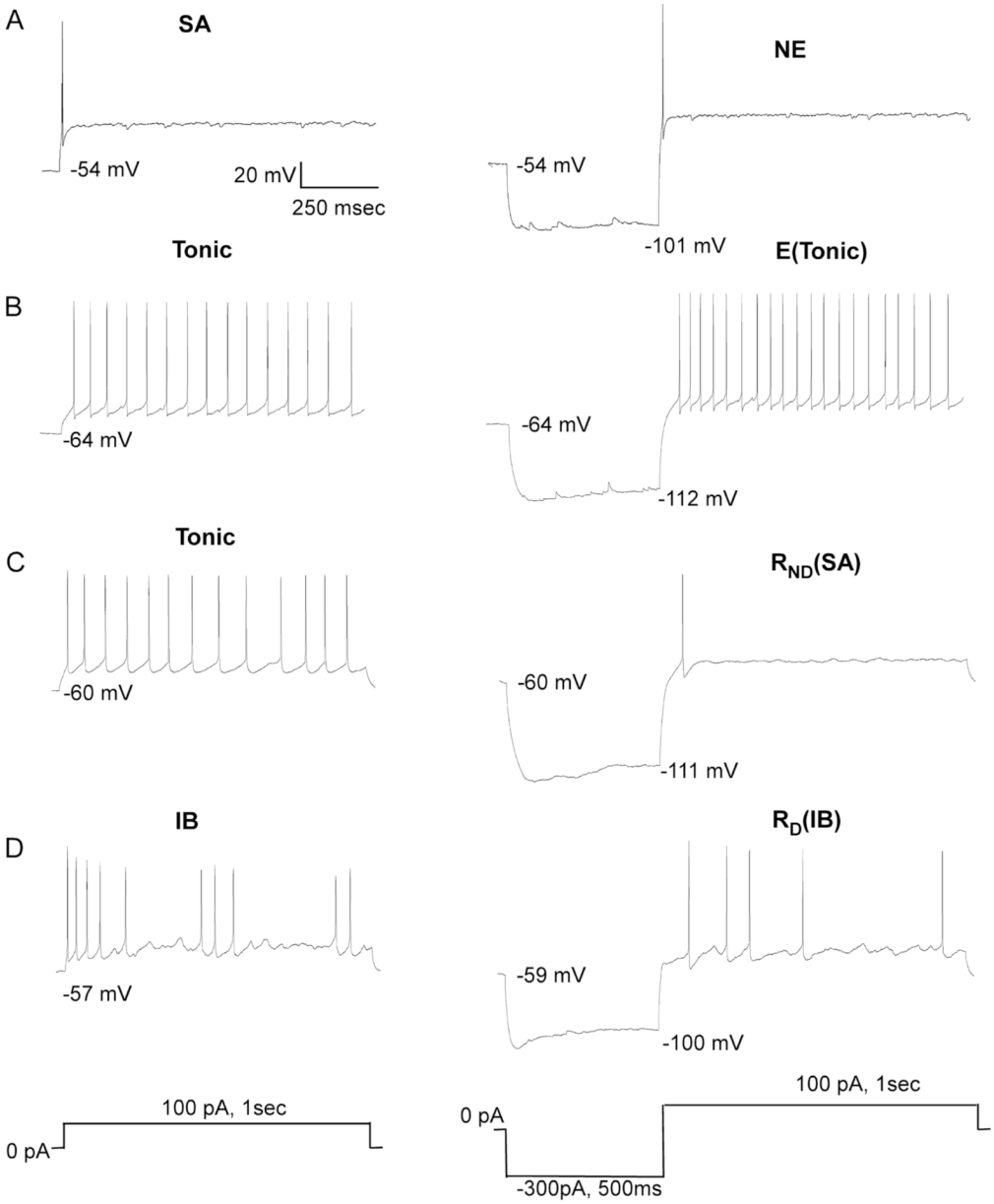

Figure 5.

Examples of each of the neuronal types with different excitability characteristics. Each row depicts the response of a neuron to depolarization (left) and the change in response with a hyperpolarizing pre-pulse (right). A. Spike adaptive (SA) neuron shows no effect (NE) following the pre-pulse. B. Neuron with a tonic response to depolarization. A hyperpolarizing pre-pulse induced an increase in excitability (E) but the response remained tonic. C. Another neuron with a tonic response to depolarization. A hyperpolarizing pre-pulse reduced excitability to one spike (spike-adaptive) but there was no delay (R_{ND}). D. Irregular bursting neuron (IB) with a hyperpolarization-induced delayed and reduced response (R_D) that remained irregular.

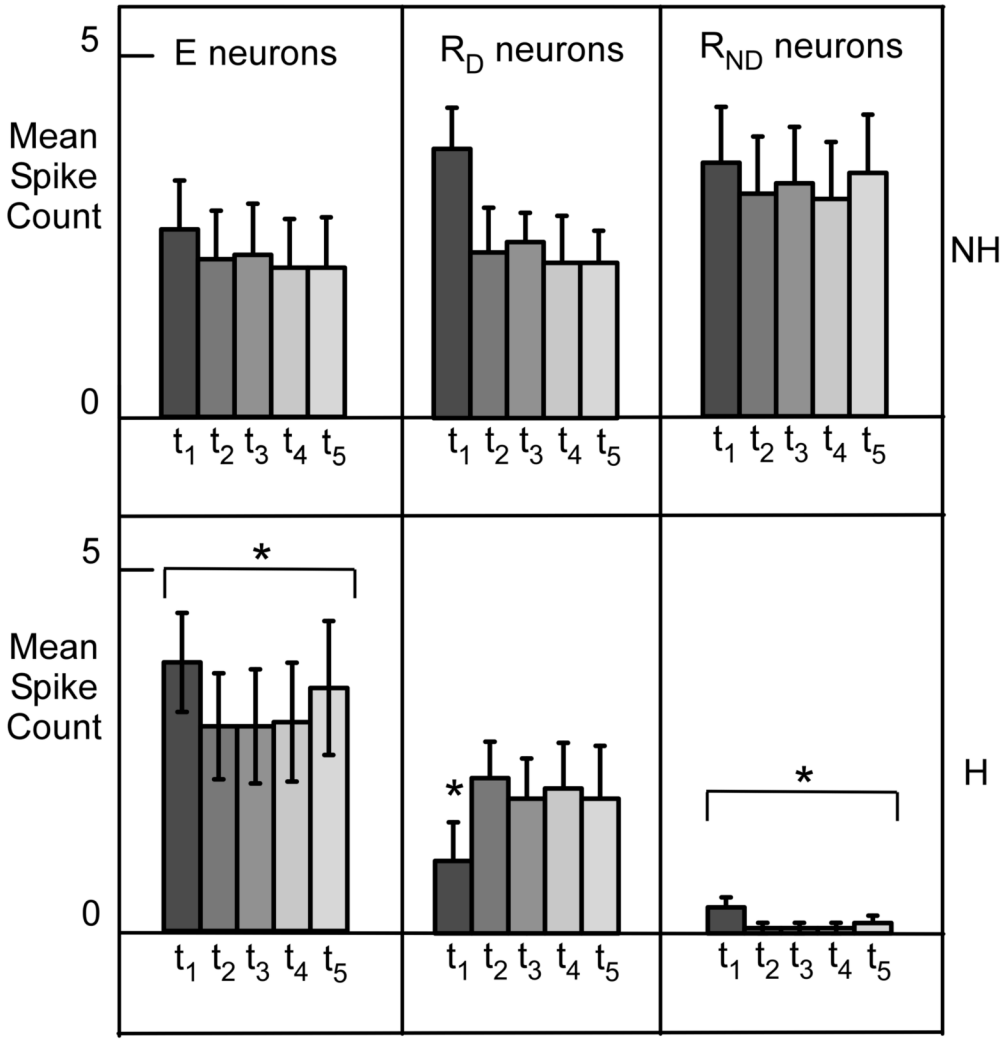

Figure 6.

Top: Mean spike counts for 3 categories of neurons as a function of time (200 ms successive intervals) to 1s depolarization without (top) and with (bottom) a hyperpolarizing pre-pulse. Abbreviations: E, neurons with increased excitability; R_D, neurons with reduced excitability and a delay to the first action potential; R_{ND}, neurons with reduced excitability without a delay in the first action potential; NH, no pre-hyperpolarization; H, with pre-hyperpolarization. Error bars indicate standard error of the mean.

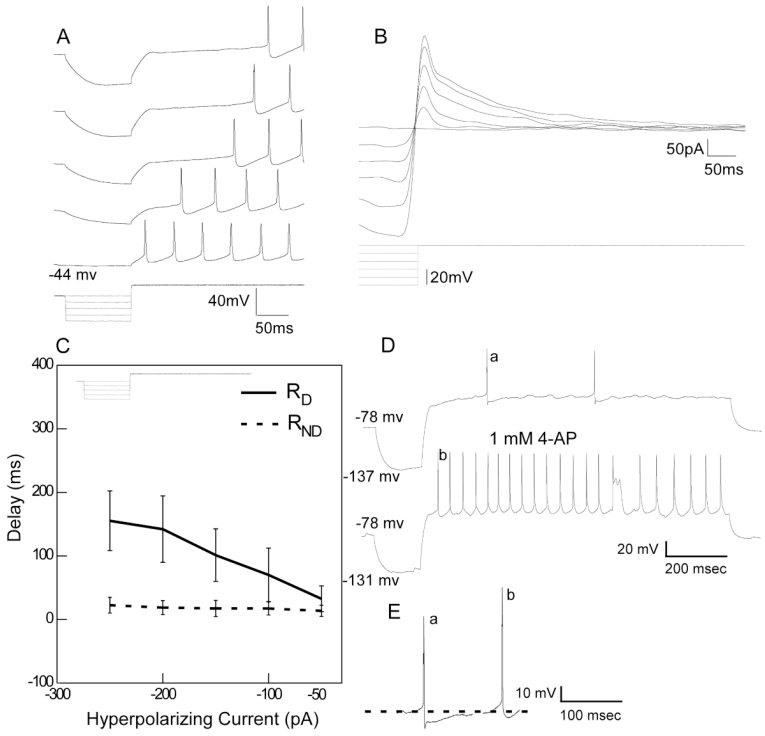

Figure 7.

A. R_D neuron showing a delay in spike onset with increasing levels of pre-pulse hyperpolarization. B. Under voltage-clamp the same neuron shows a transient outward current that increases at higher levels of hyperpolarization. C. Mean responses of the relationship between spike delay and hyperpolarizing current for 5 R_D and 5 R_{ND} neurons. D. Delay is reduced in the presence of 4-AP. E. In addition to the effects on delay and the increase in neural spike discharge, 4-AP reduced the after-hyperpolarization following each action potential. a. first action potential shown in D top trace, b. first action potential in D, bottom trace. Note also the increase in the overshoot of the action potential from 13.32 mv (a) to 21.32 mv (b).

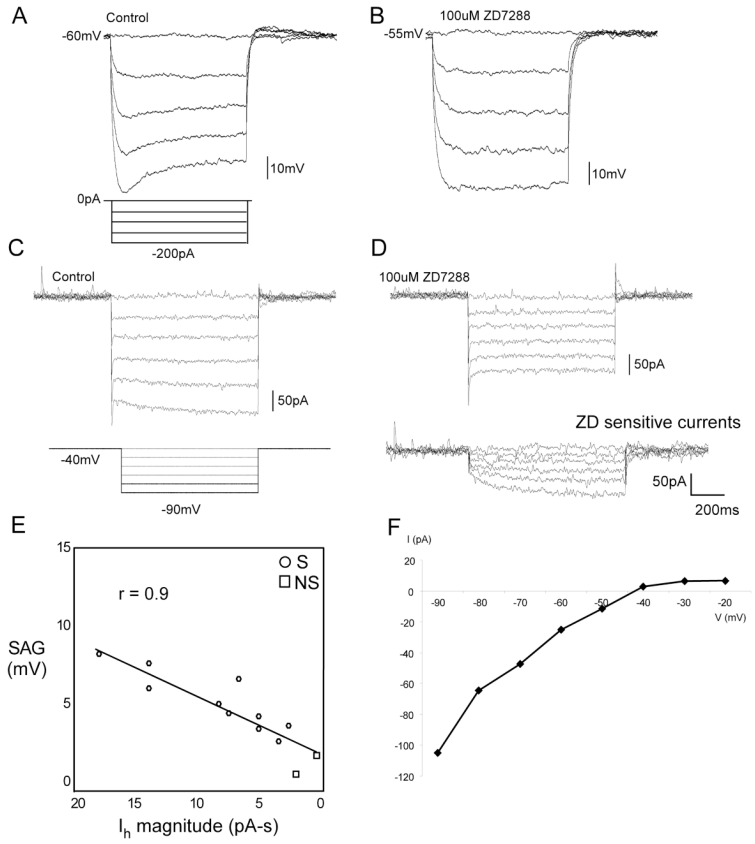

Figure 8.

A. Current-clamp recording demonstrating hyperpolarization sensitive membrane voltage sag that is suppressed by ZD7288 (B). C. Voltage-clamp recordings from the same neuron illustrating slow inward currents at greater hyperpolarization that are similarly suppressed by the non-specific cation blocker ZD7288; note digitally subtracted ZD-sensitive currents (D). E. Linear regression for membrane sag versus magnitude of slow inward current; note that the two cells with no sag (NS) had the least slow inward current. F. I-V plot of the ZD-sensitive currents indicating a reversal potential of −42.5 mV for the mixed cation current I_h.

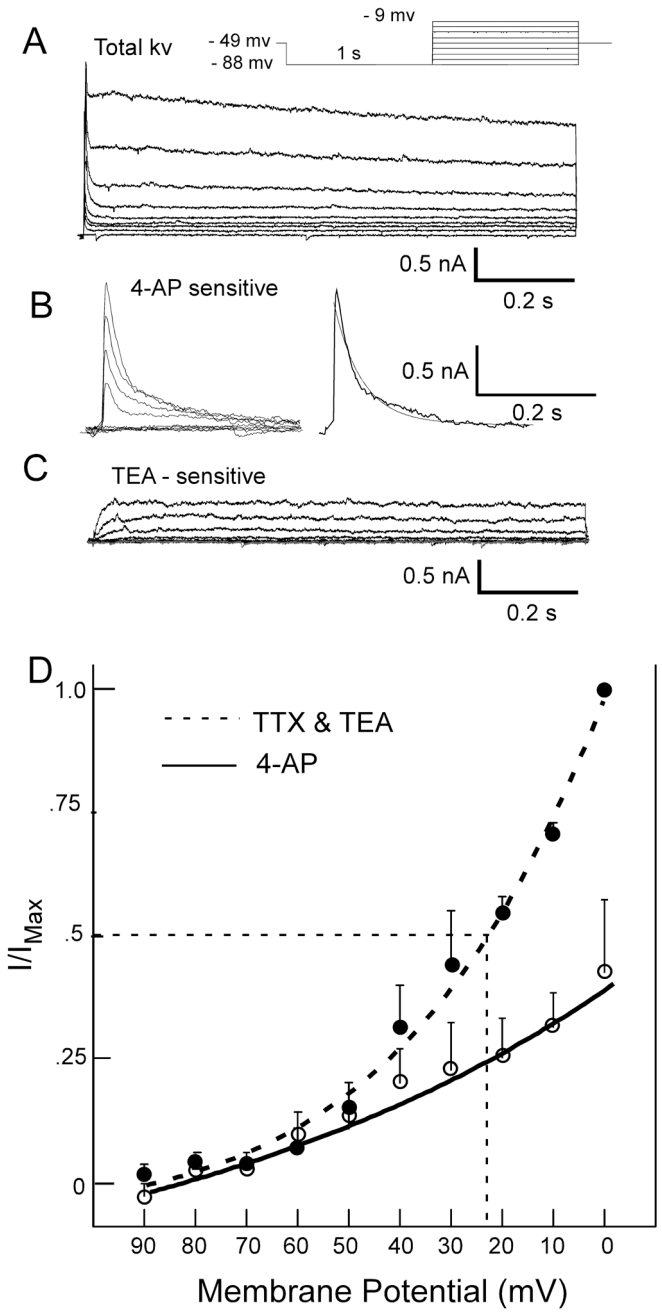

Figure 9.

A. Total outward current evoked by depolarization preceded by a hyperpolarizing pre-pulse (protocol in inset). B. A 4-AP sensitive current was derived by subtracting the current obtained in the presence of 4-AP (4-AP resistant: not shown) from the total current shown in A. The transient 4-AP sensitive outward current was fit with a dual expontential (smooth line): Tau 1 = 85 ms, Tau 2 = 4.8 ms. C. A sustained, non-inactivating current was evident by subtracting the current obtained in the presence of TEA (TEA resistant) from the 4-AP resistant current. D. Peak transient outward current as a function of membrane voltage fit with a Boltzmann curve (n=3).

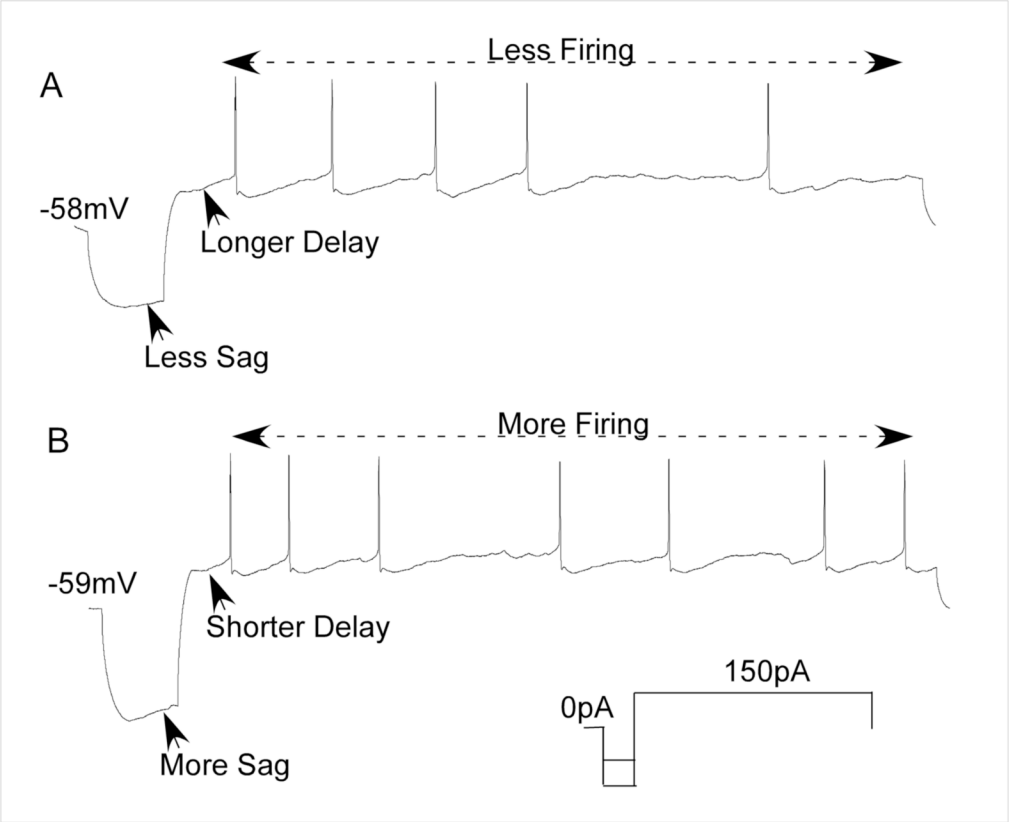

Figure 10.

A. Current-clamp recording from a delay neuron. A. Effects of a 200pA hyperpolarizing pre-pulse. B. Effects of a 300pA hyperpolarizing pre-pulse. A larger sag during depolarization following a −300pA current injection (bottom) is associated with a shorter delay compared to a −200 pA hyperpolarization that produced less sag and longer delay. Note that the number of spikes was greater with larger sag and lower with increased delay, suggesting an interaction between I_h and I_A.

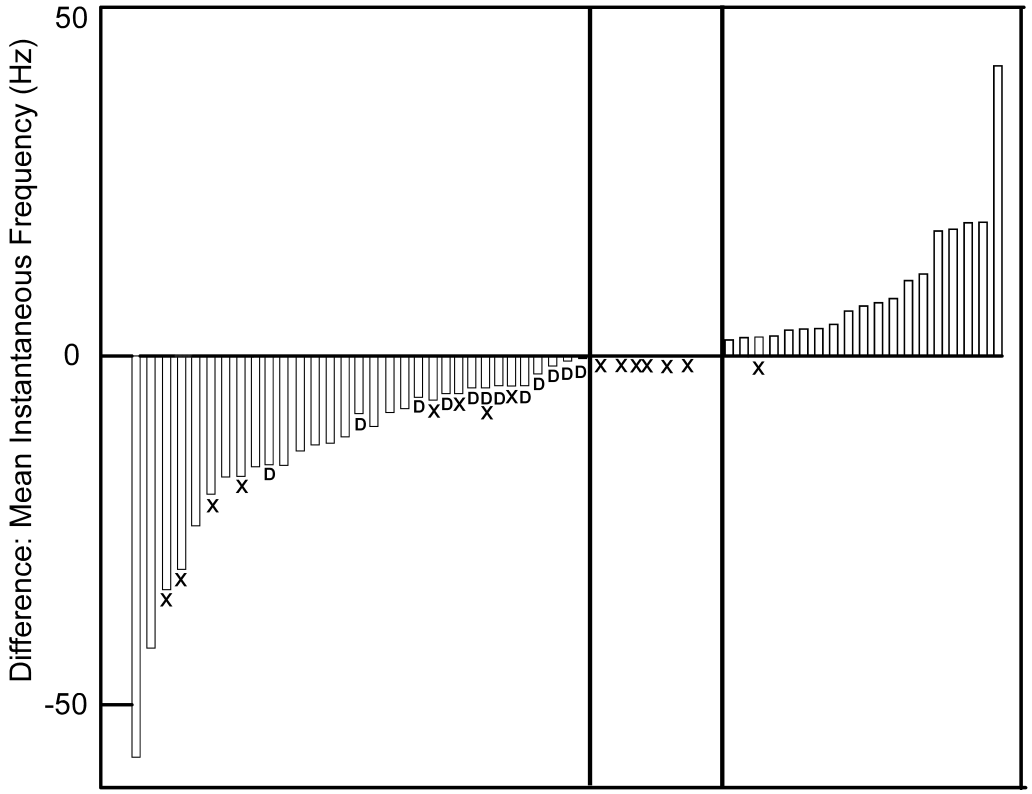

Figure 11.

Fifty neurons are rank ordered for their change in excitability defined as the difference between the mean instantaneous frequency (MIF) in spike trains obtained by membrane depolarization with and without a hyperpolarizing pre-pulse. Blue bars represent R_{ND} cells with reduced MIF. Red bars E cells with increased MIF. Open bars indicate the subset of R_D neurons with delay. Eleven neurons had no change in excitability (NE) (middle panel). Hatching (or "X's") indicates neurons without membrane voltage sag. Note that all but one neuron with increased MIF had sag compared to 8 R neurons and 6 no change neurons.

Table 1

Properties of neurons classified morphometrically

	Fusiform (12)	Pyramidal (6)	Multipolar (18)
RMP (mV)	−56 ± 2.63	−56.8 ± 3.01	−52.4 ± 2.28
Input Res. (MΩ)	232 ± 18.29	214.2 ± 39.52	231.6 ± 28.12
Time Constant (msec)	2.15 ± 0.4	2.74 ± 1.65	1.66 ± 0.253
Max Sag (mV)	9.4 ± 1.62	11 ± 4.02	6.53 ± 1.83
Area (μM^3)	171.5 ± 21.36	249.3 ± 49.71	176.2 ± 26.71
Form Factor	.64 ± 0.042[a,b]	.69 ± 0.06	.74 ± 0.03[a,b]
Primary dendrites	2.75 ± 0.025	3.33 ± 0.33	4 ± 0.3
dendritic length (μM)	1696.4 ± 245	1466.1 ± 197.3	1268.3 ± 158.03

[a]: p<.03 Fisher's Least Square

[b]: p< .004 Fischer's Least Square

Table 2

Neuron types: depolarization versus hyperpolarizing pre-pulse

Depol: *pattern*	**Tonic 39**							**IB 12**				**SA 11**
Hyper/Depol *excitability*	E 14		R_D 10		R_{ND} 15			E 5		R_D 2	R_{ND} 5	NE 11
Hyper/Depol *pattern*	Tonic 13	IB 1	Tonic 9	IB 1	Tonic 2	IB 6	SA 7	Tonic 1	IB 4	IB 2	SA 5	SA 11

Action potential firing patterns: Tonic, Irregular/burst (IB), spike-adaptive (SA)

Hyperpolatization-induced excitability changes: increased spiking (E), reduced spiking (R) with delay R_D or no-delay R_{ND}, no effect (NE).

Table 3

Properties of neurons classified by change in excitability

	Excited (E) 19	Reduced (R) 32	No Effect (NE) 11
RMP (mV)	−54.3 ± 2.1	−57.5 ± 1.8	−59.6 ± 1.88
Input Res. (MΩ)	249.8 ± 29.7[b]	218.8 ± 17.27	159.7 ± 11.26[b]
Time Constant (msec)	2.4 ± 0.64[c]	1.46 ± 0.17	0.88 ± 0.26[c]
Max Sag (mV)	10.3 ± 2.16[a]	7.5 ± 1.2[a]	2.7 ± 0.91[a]
Area (μM^3)	144.8 ± 11	202.7 ± 27.92	247.8 ± 66.37
Form Factor	.71 ± 0.03	.69 ± 0.04	.69 ± 0.1
Primary dendrites	3.5 ± 0.4	3.3 ± .22	4.3 ± 0.75
dendritic length (μM)	1500.6 ± 217.5	1490.9 ± 165.4	1037.1 ± 219.13

[a]: p< .01 Fisher's Least Square

[b]: p<.02 Fisher's Least Square

[c]: p <.01 Fisher's Least Square